ACS APPLIED BIO MATERIALS

www.acsabm.org

Article

Self-Assembled Oleic Acid-Modified Polyallylamines for Improved siRNA Transfection Efficiency and Lower Cytotoxicity

Cristian Salvador, Patrizia Andreozzi, Gabriela Romero, Iraida Loinaz, Damien Dupin,* and Sergio E. Moya*

Cite This: *ACS Appl. Bio Mater.* 2023, 6, 529−542

Read Online

ACCESS | Metrics & More | Article Recommendations | Supporting Information

ABSTRACT: Small interference RNA (siRNA) is a tool for gene modulation, which can silence any gene involved in genetic disorders. The potential of this therapeutic tool is hampered by RNA instability in the blood stream and difficulties to reach the cytosol. Polyamine-based nanoparticles play an important role in gene delivery. Polyallylamine hydrochloride (PAH) is a polycation displaying primary amines that can be easily chemically modified to match the balance between cell viability and siRNA transfection. In this work, PAH has been covalently functionalized with oleic acid at different molar ratios by carbodiimide chemistry. The substituted polymers form polyplexes that keep positive surface charge and fully encapsulate siRNA. Oleic acid substitution improves cell viability in the pulmonary cell line A549. Moreover, 6 and 14% of oleic acid substitution show an improvement in siRNA transfection efficiency. CD47 is a ubiquitous protein which acts as "don't eat me signal." SIRPα protein of macrophages recognizes CD47, leading to tumor cell phagocytosis by macrophages. By knocking down CD47 with siRNA, cancer cells become vulnerable to be eliminated by the immune system. PAH−oleic acid substitutes show high efficacy in silencing the CD47 protein, making them a potential candidate for immunotherapy.

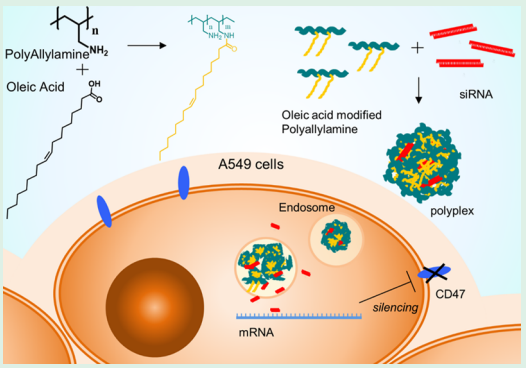

KEYWORDS: *siRNA delivery, polyallylamine hydrochloride, polymeric nanoparticles, oleic acid, CD47*

1. INTRODUCTION

RNA interference is a natural pathway occurring in the cell cytosol that regulates endogenous gene expression and protects cells from exogenous nucleic acids. It is triggered by any double-stranded RNA, and its outcome is the knockdown of specific genes.[1] This pathway involves microRNA (miRNA) and small interference RNA (siRNA), which bind sequence-specific to mRNA, resulting in the degradation of gene-specific mRNA.[2] siRNAs and miRNAs can be artificially synthesized to target any therapeutically interesting gene and hamper its expression.[1,3] It has a great therapeutic potential to treat any disease provoked by the malfunction of a gene and has several advantages over small molecules and monoclonal antibody therapies.[4] Considerable efforts have been made since the discovery of RNA interference in 1998[5] that made possible in 2018 the approvement by the FDA of the first medicament based on siRNA therapy. Onpattro, produced by Alnylam Pharmaceuticals, is the first RNAi drug for the treatment of hereditary transthyretin-mediated amyloidosis with polyneuropathy in adults.[6] In 2019, the FDA also approved GIVLAARI against acute hepatic porphyria.[7,8]

Despite the promising and powerful therapeutic outcomes offered by siRNA technology, some drawbacks still hamper its clinical translation. siRNAs cannot be systemically administered because they are degraded by endonucleases.[9] In addition, siRNA is 7−8 nm long, with a 2−3 nm diameter and a molecular weight of 13−16 kDa displaying negative charges,[4] which make siRNA easily cleared out instead of accumulating in targeted tissues.[10] Fenestrated vessels, such as in liver, are the most common final destination of siRNA, which ends up being eliminated through the gallbladder to the intestine.[11,12] Moreover, at the cellular level, free siRNAs cannot escape the endosome and translocate into the cytosol, where they must act.

Several delivery platforms have been developed to overcome all these limitations and effectively deliver siRNAs in their site of action.[13] siRNA nanoformulations aim at overcoming biological barriers, ensuring that siRNAs are protected from endonucleases. Clearance occurs in the glomerulus. The glomerulus pore has a diameter of around 8 nm, and thus larger particles entrapping siRNA avoid its filtration through the kidneys. Carriers that are not cleared, degraded, or phagocytosed leave the endothelium to reach target tissues.

Received: October 2, 2022
Accepted: December 4, 2022
Published: January 17, 2023

Most carriers cross the cell membranes by endocytosis, and endocytic vesicles fuse with early endosomes and become acidic in the inner environment.[14,15] Some of these nanocarriers, like cationic lipids and/or polymers, protonate at endosomal pH. Low pH triggers disruption of the endosomal membrane by complexation with negatively charged lipids or by creating an osmotic difference with the cytosol, which results in their translocation and the release of the siRNA in the cell cytoplasm.[14]

Several nanomaterials have been used for siRNA delivery like lipid nanoparticles,[16] polymer nanoparticles,[17] exosomes,[18] aptamers,[19] and inorganic nanoparticles.[13,20] Cationic polyelectrolytes and lipids are without any doubt the most efficient in complexing siRNAs through their positive charges via electrostatic interactions. However, positive charges induce toxicological endpoints over a certain concentration, limiting the therapeutic outcome. Therefore, it is critical to have control on the density of positive charges in the carriers, which are needed for complexation and translocation but are sources of toxicity as well. There are some fundamental differences between polyelectrolytes and lipids for siRNA complexation. Polyelectrolytes interact with nucleic acids at several charged groups per polymer chain, whereas lipids have a more labile binding with nucleic acid. The lipid-siRNA complex is easier to break, and lipids have a greater capacity for reorganization during translocation in the cytoplasm. Lipids can also fuse with endosomatic membranes, facilitating translocation in the cytoplasm.[21] Aliphatic lipid chains also help in the encapsulation of nucleic acids. In fact, charged lipids have been shown to be more efficient at encapsulating nucleic acids than polyelectrolytes. However, polycations have more loading capacity and are more likely to induce osmotic swelling within the endosomes, triggering endosomal escape. An ideal carrier for siRNA delivery would combine characteristics of both polycations and cationic lipids. In the literature, we can find reports on polyethylenimine (PEI) modification with lipids to form the so-called lipopolyplexes. Lipopolyplexes show an enhanced transfection efficiency coming from the combination of the polymers with lipids and a reduced cytotoxicity.[22] In some reports, liposomes are prepared with an inner core of PEI.[23−25] However, the most common approach is to modify the backbone of PEI with aliphatic chains.[26,27] Long aliphatic chains of C18 carbons, that is, stearic, linoleic, and oleic acid (OA), resulted in better performance than shorter C8 and C14 aliphatic chains, that is, caprylic and myristic acids.[28,29]

Efforts have been made toward bringing new siRNA-based therapies against cell lung cancer (NSCLC) by targeting oncogenes related to tumor angiogenesis (VEGF), tumorgenesis downstream pathways (KRAS), and tumor maintenance proteins that confer resistance to chemotherapy (BCL2).[30] Some therapies involve reprograming immunogenic cells toward cancerous cells, such as T lymphocytes,[31] natural killers,[32] and tumor-associated macrophages.[33] Another interesting strategy is to modify tumor cells for being eliminated by macrophages.[34]

CD47 is a transmembrane protein ubiquitously expressed in normal cells and overexpressed in cancer cells. CD47 acts as a "don't eat me signal," It is recognized by signal regulatory protein α (SIRPα) expressed in macrophages promoting the inhibition of phagocytosis. CD47 labels cells permitting macrophages distinguishing between "native" and "foreign" cells, where stronger cells are deleted by engulfment. Mutant genes in NSCLC and in other types of cancers overexpress CD47. Knocking down the levels of CD47 in lung tumors is a promising approach to treat NSCLC. Recent studies have demonstrated the efficacy of blocking SIRPa/CD47 interactions with anti-CD47 antibodies.[34,35] Few papers have studied the knockdown of CD47 in melanoma,[36] ovarian cancer,[35] and lung cancer[37] by using siRNA therapy.

The aim of this work is to combine polyamines with C18 aliphatic chain to create a vector nanoparticle for complexation of siRNA with enhanced silencing efficiency and low toxicity that benefit from advantageous properties of both lipids and polymers. Polyallylamine hydrochloride (PAH), a polycation displaying primary amines, has been conjugated with OA through carbodiimide chemistry. In previous work, we have shown that PAH/siRNA complexes disassemble at endosomal pHs releasing the siRNA, while they are very stable at physiological pHs, and they are also toxic at relatively low polymer concentrations. By combining PAH with lipids, we will be able to control charge density and modulate toxicity but retaining the advantages of primary amines for siRNA delivery.[38] Here, we show for the first time that the OA-modified PAH results in a promising nanoparticle carrier for siRNA delivery, and we test its capacity in immunotherapy for knocking down the CD47 protein.

2. MATERIALS AND METHODS

2.1. Materials. All materials used in the experimental section are described in the Supporting Information.

2.2. Synthesis and Characterization of Oleic Acid-Substituted Polyallylamine. PAH of 17.5 kDa was substituted covalently with OA via the carbodiimide/N-hydroxysuccinimide reaction. Different molar ratios of $-NH_2/-COOH$ were tested: 1:0.01, 1:0.02, 1:0.05, 1:0.1, and 1:0.2, hereafter named PAH.OA.1, PAH.OA.2, PAH.OA.5, PAH.OA.10, and PAH.OA.20. The corresponding molar amounts of OA were dissolved in 48 mL of DMSO. 3-Ethylcarbodiimide hydrochloride (EDC) and *N*-hydroxysuccinimide (NHS) were added to the OA solution at 10:10:1 molar ratio of EDC/NHS/−COOH. The solution was stirred at 37 °C for 30 min to achieve preactivated NHS esters of OA. 100 mg of PAH was dissolved in 12 mL of deionized water (diH_2O) and added dropwise to the DMSO solution during 1 h. The mixture of water/DMSO was stirred for 72 h at 37 °C. The polymer was purified by dialysis against diH_2O for 10 days, changing diH_2O twice a day. Finally, the dialyzed aqueous solution was freeze-dried until obtaining a white cottonlike powder. Free OA presence was assessed by thin-layer chromatography (TLC). The degree of OA substitution was determined by ^{1}H NMR (500 MHz D_2O): δ ppm 0.8 (m, $-CH_3$ oleyl), 1.1−1.5 (m, $-CH_2$ oleyl and PAH), 1.5−2.1(m, $-CH_2-CH_2-CO-N$, oleyl; $-CH_2-CH{=}CH$ Oleyl; −CH− PAH; $-CH_2-CO-N$, Oleyl), 2.8−3.3 (s, $-CH_2-N$), 5.5 (s, $-CH{=}CH-$). The degree of substitution for the different ratios of amines to lipids employed was evaluated comparing the methyl protons of the oleyl chain at δ 0.8 and multiplet at δ 2.8−3.3. The OA-substituted polymers obtained were named as the original amount of OA added to the reaction: PAH, PAH.OA.1, PAH.OA.2, PAH.OA.5, PAH.OA.10, and PAH.OA.20.

2.3. Preparation of siRNA/Polymer Polyplexes. siRNA/polymer complexation was performed for the following N/P ratios: 2.5, 5, 10, and 15. The N/P ratio is defined as the moles of nitrogen present in the polymer divided by moles of phosphates in the siRNA. The corresponding amount of the polymer was dissolved in 50 μL of RNAse-free water to achieve the desired N/P ratio. The corresponding amount of siRNA was added to polymer aqueous solution and then mixed by pipetting up-down or by a short vortex. Samples were incubated for 15 min at room temperature (RT) to allow both molecules to form complexes.

2.4. Size by DLS and *Z*-Potential. Freeze-dried samples were dissolved in diH_2O with the help of vortex and a sonication bath. Samples were diluted until achieving a 100 μg/mL concentration in

https://doi.org/10.1021/acsabm.2c00845
ACS Appl. Bio Mater. 2023, 6, 529−542

200 μL of diH_2O and filtered through 0.44 μm filters. Polyplexes at different N/P ratios of 2.5, 5, 10, and 15 were formed as described above, scaling-up to 200 μL and filtering through 0.44 μm. Dynamic light scattering (DLS) measurements were conducted in a disposable low volume cuvette (BRAND UV cuvette micro-7592) and zeta potential in DTS1070 cuvettes. DLS and aqueous electrophoresis measurements were performed in a Zetasizer nano ZS ZEN3600 model (Malvern Instruments Ltd.) at a laser wavelength of 633 nm and a scattering angle of 173° to obtain the hydrodynamic diameter and *Z*-potential.

2.5. Transmission Electron Microscopy. Free polymer and polyplexes were prepared at a final concentration of 100 μg/mL polymer in RNAse-free diH_2O. Samples were filtered through 0.44 μm filters, and 5 μL were transferred onto a carbon film coated copper grid (400 mesh), previously hydrophilized by glow discharge. After 5 min of incubation, the solution was removed with a filter paper. Samples were negatively stained with 5 μL of ammonium molybdate pH 7, 12% w/v by 5 min incubation. Grids were washed with diH_2O and overnight dried before being measured. Transmission electron microscopy measurements were performed with a JEOL JEM 1010 microscope operating at an acceleration voltage of 100 kV.

2.6. Quant-IT Ribogreen. Quant-IT ribogreen assay was used to quantify siRNA encapsulation. Quant-IT ribogreen is a fluorophore which binds to siRNA and other nucleic acids when these are free in solution but not when they are complexed as in polyplexes. siRNA-polyplexes at four different N/P ratios were made as described above. Then, the protocol provided by the manufacturer was followed for two groups: untreated and treated with heparine. Fluorescence was measured exciting at 480 nm and emitting at 520 nm in a fluorescence plate reader Synergy HT by Biotek. Then, the encapsulation efficiency was calculated as follows

$$\text{Encapsulation efficiency EE (\%)} = 100 - (((U_{\text{sample}} - U_{\text{blank}})/((T_{\text{sample}} - T_{\text{blank}}) \times 100$$

U = untreated; T = treated with Heparin solution.

2.7. Cell Culture. A549 human pulmonary cell line was cultured with Eagle minimum essential medium (EMEM) supplemented with 10% v/v fetal bovine serum (FBS) and 1% v/v penicillin−streptomycin (P/S). A549 stably expressing eGFP (A549-GFP) were kept in EMEM medium supplemented with 10% FBS, 1% P/S, and 10 μg/mL blasticidin.

2.8. Cytotoxicity Assay: MTS and Live/Dead. Cytotoxicity of polyplexes was evaluated for the A549 cell line after 24 h exposition. The cells were seeded in a 96-well plate using EMEM supplemented with 10% FBS and 1% P/Sand incubated for 24 h. When the cells were confluent, polyplexes were added to the cell culture freshly prepared as described above. PAH, PAH.OA.1, PAH.OA.2, PAH.OA.5, PAH.OA.10, and PAH.OA.20 at four different N/P ratios were tested, with a final siRNA concentration of 200 nM per well. Medium was replaced in each well with OptiMEM reduced serum medium, and polyplexes were added to the well in four technical replicates. After 24 h of incubation at 37 °C, and 5% CO_2 MTS CellTiter 96 Aqueous One solution or live/dead test was conducted. A corresponding volume of MTS solution was added to each well and incubated for 2 h at 37 °C and 5% CO_2. Absorbance of the formazan resulting product was measured at 490 nm in a Synergy HT plate reader by Biotek.

For live/dead, kit components Calcein AM and ethidium homodimer-1 were diluted in cell medium to recommended working concentrations of 2 and 4 μM, respectively. Solution was added to the wells, and the plate was incubated 45 min at room temperature. Right after, the cells were washed and observed under a microscope.

2.9. Polymer Labelling with Fluorophore Atto-633. Fluorophore Atto-633-NHS ester was attached to PAH, PAH.OA.1, PAH.OA.2, PAH.OA.5, PAH.OA.10, and PAH.OA.20 following provider's instructions, with a few modifications. Labelling was performed adding 1 molecule Atto-633 per 2000 monomers of the polymer. Between 5 and 8 mg of different polymers and 0.02 mg of Atto-633 were used. The polymers were dissolved in 2 mL of diH_2O, and pH was adjusted to about 8. A solution of 20 μL of Atto-633 in DMF was added to the polymer solution. The Reaction was stirred for 2 h protected from light. The reaction product was purified by PD-10 desalting columns and dialysis in a Floatlyzer G2 2.5−5 kDa against water for 2 days. Samples were freeze-dried and analyzed by ^{1}H NMR (500 MHz D_2O) and fluorescence correlation spectroscopy (FCS) to verify that the entire dye was attached to the polymer.

2.10. Cell Uptake Studies. A549 cells were cultured in 8-well ibidi plates at 30.000 cell/well. 24 h after, polymers labeled with Atto-633 (PAH, PAH.OA.1, PAH.OA.2, PAH.OA.5, PAH.OA.10, and PAH.OA.20) were used to form polyplexes with siRNA-6-FAM at ratio N/P 5 as described above. The final concentration of siRNA per well was 200 nM. The resulting polyplexes were exposed to confluent cells for 24 h for transfection. Then, the cells were washed with DPBS, fixed with 4% v/v paraformaldehyde (PFA), and permeabilized with 0.5% v/v Triton-X-100, washing with DPBS between steps. After that, the cell nucleus was stained with dilution of 1:2000 Hoechst 33342 and actin with ActinRedTM 555. Fixed cells ready for imaging were embedded in DPBS. Ibidi plates were set up using confocal laser scanning microscopy (CLSM, Zeiss LSM 510). CLSM images were acquired by exciting at 405, 488, 56,1 and 633 nm laser lines, with a 63× objective. *Z*-stack experiments were also performed and displayed as orthogonal view processed by ZEN 3.3 software and ImageJ.

Quantification of siRNA-6-FAM internalization by flow cytometry was carried out as follows. 60.000 cells/well A549 cells were seeded in a 24-well plate. After 24 h, polyplexes were formed at N/P 5 with different polymer substitutions and siRNA-6-FAM, keeping a final concentration of siRNA at 200 nM per well in every condition. Polyplexes were exposed to confluent cells embedded in OptiMEM media. After 24 h of incubation, the cells were washed and lifted with 0.25% trypsin/ethylenediamine tetraacetic acid (EDTA) without phenol red. Trypsin was blocked by adding DPBS 10% FBS, and the resulting cell containing solution was transferred to a flow cytometry tube. 10,000 events were measured using FACS diva Canto II software. Data are showed as percentage of events that have 6-FAM fluorescence. Setting parameters as nontreated cells present 0% of fluorescence.

2.11. Delivery Efficiency by Flow Cytometry. Delivery efficiency of siRNA inside cells was assessed by measuring the siRNA silencing of the GFP protein by flow cytometry. A549 cells stably expressing eGFP (A549-GFP) were seeded in 24-well plates at 60,000 cells/well using EMEM, 10% v/v FBS, 1% v/v P/S, and 10 μg/mL blasticidin. Transfection was performed using polyplexes of PAH.OA/siRNA anti-eGFP at ratios N/P 2.5, 5, and 10 using 0.1 nmol of siRNA to achieve a final concentration of 200 nM per well. Lipofectamine RNAimax was used as the positive control, and the complex was prepared following the protocol provided by the manufacturer using the same amount of siRNA. Cell media were substituted by OptiMEM, and complexes were distributed into the well. After 24 h of incubation, the cells were washed and refreshed with growth media. The cells were incubated between 72 and 96 h after transfection to obtain an effective protein reduction. Once incubation was finished, the cells were lifted with 0.25% trypsin/EDTA without phenol red. Trypsin effect was blocked with DPBS and10% FBS, and the resulting cells solution was transferred to a flow cytometer's tube. Samples were measured with a FACS diva canto II flow cytometer. FITC filter was applied to count GFP-expressing cells. Software BD FACS Diva was used to measure the mean fluorescence intensity of 10,000 events per condition. Data are presented as relative GFP expression normalized to the intensity of the nontreated cells, considered 100% of GFP-expression. Every condition had 2 technical replicates.

2.12. mRNA Quantification by RT-qPCR. A549 cells were seeded in a 24-well plate at 60,000 cells/well. Four wells per condition were used. 24 h after, confluent cells were transfected with polyplexes to OptiMEM media. Polymers with different substitutions of OA were complexed with 0.1 nmol of anti-CD47 siRNA and 0.1 nmol of negative control siRNA at a ratio of N/P 5, resulting in 200 nM of final siRNA concentration per well. After 24 h, the cells were washed with DPBS and fresh growth media were added to the well for 48 and

https://doi.org/10.1021/acsabm.2c00845
ACS Appl. Bio Mater. 2023, 6, 529−542

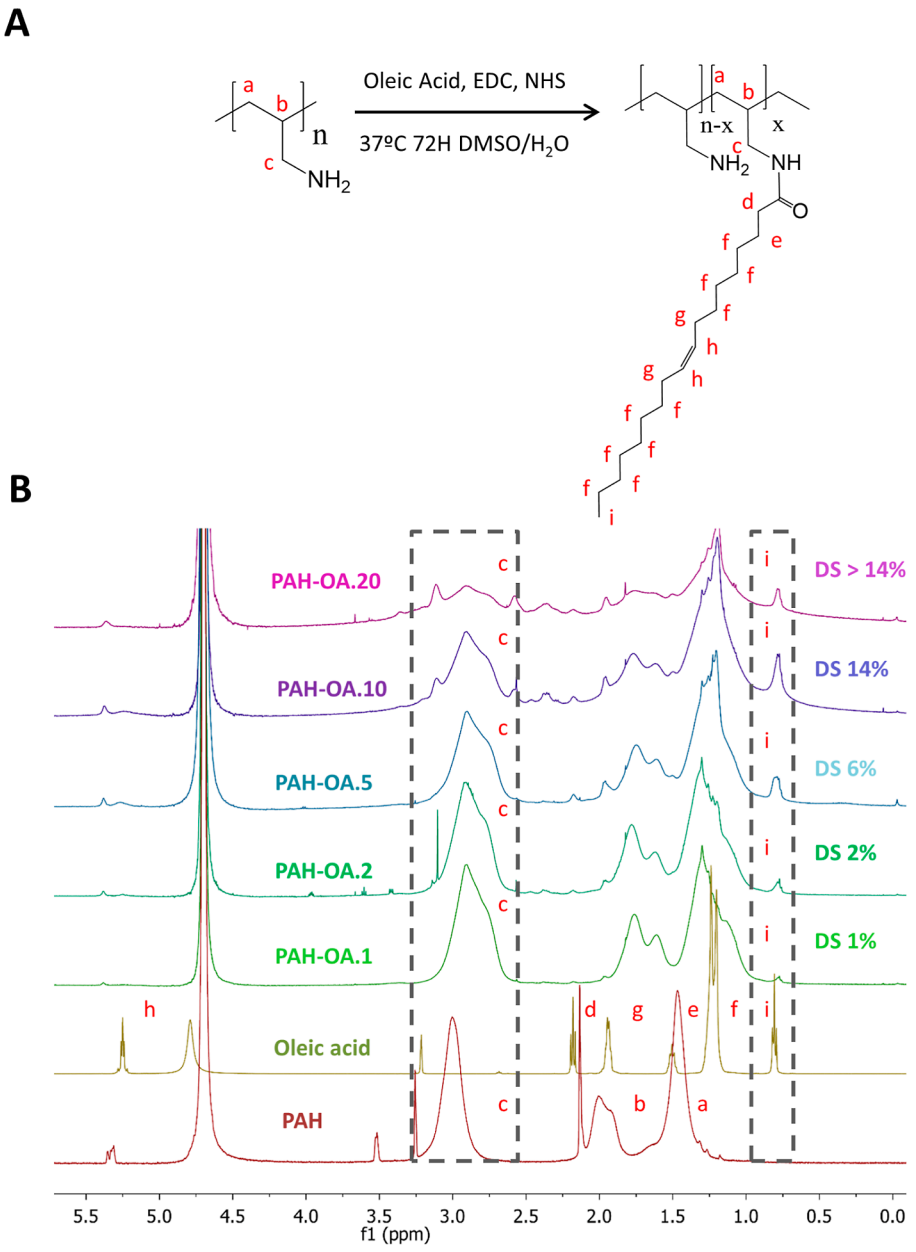

Figure 1. (A) Scheme of the reaction of Polyallylamine with OA. (B) Characterization by ^{1}H NMR spectra of PAH (D_2O), OA (MeOD) and its substitutions (D_2O). % DS was calculated by comparing integration from i and c peaks.

72 h. Levels of mRNA-CD47 were measured 24, 48, and 72 h after transfection. mRNA was extracted following the instructions of QIAGEN mini kit. Briefly, after the cells were washed, 350 μL of RLT buffer supplemented with β-mercaptoethanol was added to the wells. Wells were scratched with a pipette tip, and the solution was collected in a 2 mL tube. Solution was homogenized by passing through the needle of a syringe 5 times. The homogenized lysate was transferred to a gDNA eliminator spin column and centrifuged and flow-through was saved to the next step. 350 μL of ethanol was added to the solution, and this was transferred to the provided RNeasy spin column. The solution was centrifuged, and the flow-through was discarded. Then, RNA retained in the column was washed consecutively with buffers RW1 once and RPE twice. Finally, RNA was eluted with RNAse-free water, and the concentration was quantified with NanodropTM One. RNA obtained was transformed to cDNA using a reverse transcription system by Promega. RNA was diluted until having the same concentration for all conditions of 100 ng. Then, a master mix of $MgCl_2$, reverse transcription buffer, dNTPs, RNAsin ribonuclease inhibitor, Oligo(dT)15, and AMV reverse transcriptase was added to the RNA samples and set on a Biometra T1 thermocycler. Samples were heated 1 h at 42 °C. Once the retrotranscription finished, the samples were stored at −20 °C or directly proceeded to the next step. cDNA samples were amplified for specific gene human CD47 and the housekeeping gene human GAPDH. Bio-rad iTaq Universal SYBR green supermix was used with specific primers already designed by Bio-Rad for gene CD47. Samples of every condition were put on 96-well PCR plates by triplicates, three replicates for the target gene and three for the housekeeping gene. Plates were introduced in a Bio-Rad CFX connect Real-time PCR system. Amplification cycles were first 95 °C denatured followed by 40 cycles of 95 °C 5 s and 60 °C 30 s annealing and extension. Ct data of each sample were obtained after PCR had finished. Delta−delta Ct method ($2^{-\Delta\Delta C_t}$) was used to calculate the relative fold expression of CD47 in A549 after being transfected by siRNA anti-CD47.

2.13. Immunocytochemistry of CD47 Protein. A549 cells were cultured in 8-well ibidi plates at 30,000 cell/well. 24 h after, polymers (PAH, PAH.OA.1, PAH.OA.2, PAH.OA.5, PAH.OA.10, and

https://doi.org/10.1021/acsabm.2c00845
ACS Appl. Bio Mater. 2023, 6, 529−542

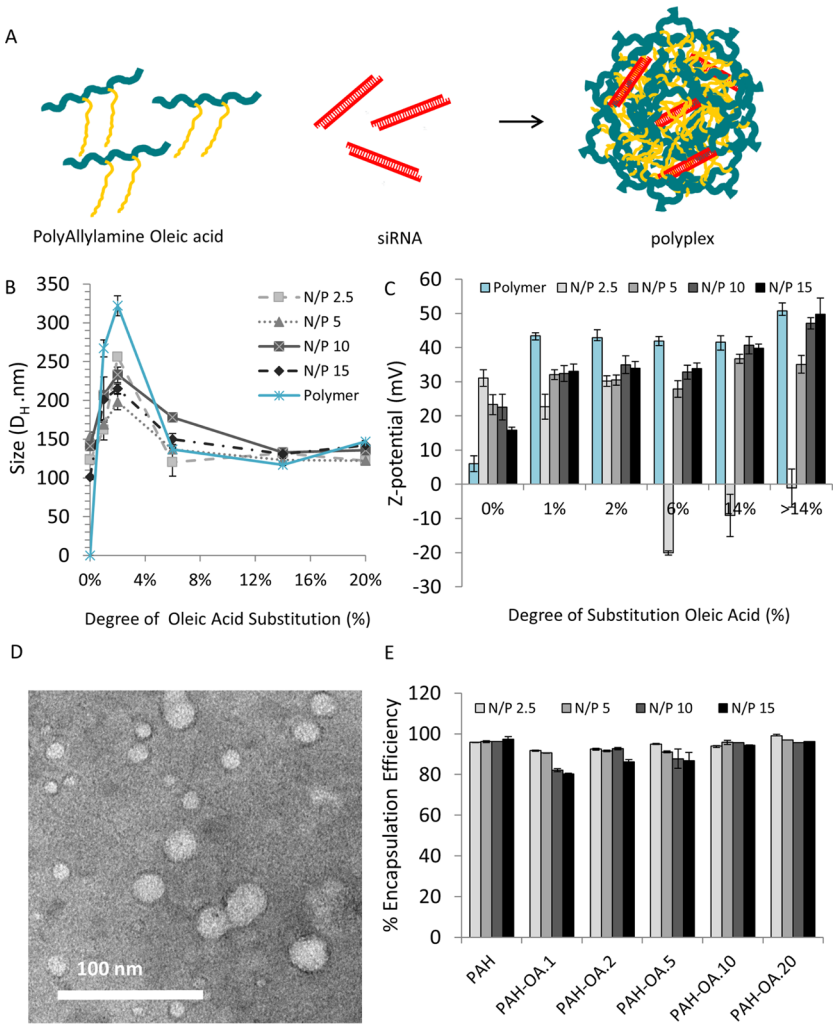

Figure 2. (A) Scheme of polyplex formation. (B) DLS measurements of polymer/siRNA polyplexes at different N/P ratios (gray scale) and free polymer (blue). Size represented in hydrodynamic diameter from the *Z*-average. (C) *Z*-potential measurements in mV of polyplexes (gray scale) and polymers (blue) in 10 mM NaCl. $n = 3$. Error bars represent standard deviation. (D) TEM images of PAH.OA.5/siRNA polyplexes dissolved and diluted 1−10 in water. Negative stained with ammonium molybdate pH 7. (E) Encapsulation efficiency of PAH and PAH.OA substitutions measured by the Quant-IT ribogreen fluorophore. Result obtained by the subtraction of h100 per cent encapsulated and not encapsulated siRNA. Not encapsulated percentage calculated by dividing free siRNA fluorescence by total siRNA fluorescence. $n = 3$. Error bars represent standard deviation.

PAH.OA.20) were used to form polyplexes with siRNA anti-CD47 and siRNA negative control both at N/P 5, keeping the concentration of siRNA at 200 nM per well. Cells were exposed to the polyplexes 24 h, and after that, they were washed and refreshed with new growth media and let the siRNA take effect up to 72 h. At this point, the cells were fixed with 4% v/v PFA and permeabilized with 0.5% v/v Triton-X-100. Cells were incubated with 5% BSA in PBST (0.1% Tween20) for 30 min at room temperature. Then, the cells were incubated with the primary antibody against CD47 overnight at 4 °C in 1% BSA PBST or only in 1% BSA PBST. Next day, the wells were washed and incubated with the secondary antibody goat against mouse FITC for 30 min at RT. Cells were washed again and incubated in a solution of 2 μg/mL Hoechst 33342 at RT for 10 min. Finally, the ibidi plate was observed using a Zeiss LSM 510 confocal laser scanning microscope at 63×x objective, and images were taken exciting cells with the 405 and 488 nm lasers.

2.14. Western Blot of CD47. A549 cell line was seeded in 56 cm^2 Petri dishes at 1,700,000 cell/dish using growth media EMEM, 10% FBS, and 1% P/S. The cells were transfected with polymer/siRNA-CD47 PAH-substituted polymers (PAH, PAH.OA.1, PAH.OA.2, PAH.OA.5, PAH.OA.10, and PAH.OA.20) and lipofectamine RNAimax as a control, having 200 nM of final siRNA concentration per Petri dish. After 72 h, the protein was extracted using 1 mL of RIPA buffer supplemented with 1% v/v phosphatase inhibitor cocktail 1, 1 mM phenylmethylsulfonyl fluoride, and 100 μL/mL protease inhibitor cocktail. Protein concentration in the supernatant was determined by the Bradford test using BSA standard. 90 μg of protein of each condition was mixed with TruPAGE LDS sample buffer (Laemmli buffer) and TruPAGE DTT sample reducer incubated at 80 °C 10 min. A 10% bis-acrylamide sodium dodecyl sulfate (SDS) gel was run in TruPAGE TEA-Tricine SDS for 30 min for stacking at 80 V and 60 min at 120 V for resolving. Once the gel was completed, proteins were transferred to a polyvinylidene fluoride membrane previously activated using a wet transfer chamber filled with cold 1× TruPAGE transfer buffer. Transfer lasted 1 h at constant 350 mA. Then, the membrane was blocked with 5% milk in TBST for 1 h at RT. After that, the membrane was treated with primary antibodies. Dilution 1/500 of CD47 in 5% milk TBST and 1/2000 of cyclophilin A (CPA) overnight at 4 °C was done while stirring in a roller mixer. Next day, 3× washes were performed with TBST before incubation with the secondary antibodies 1/2000 goat-anti-mouse-HRP for CD47 and 1/2000 goat-anti-rabbit-HRP for CPA 1 h at RT. Finally, the electrochemiluminescence substrate was applied to the mem-

https://doi.org/10.1021/acsabm.2c00845
ACS Appl. Bio Mater. 2023, 6, 529−542

brane, and chemiluminescence was revealed by a iBright imaging system.

2.15. Flow Cytometry Evaluation of CD47 Knockdown. A549 cells were cultured in a 24-well plate at 60,000 cells/well in growth media EMEM, 10% FBS, and 1% P/S. 24 h after, the cells were transfected with polyplexes formed with different polymers PAH, PAH.OA.1, PAH.OA.2, PAH.OA.5, PAH.OA.10, PAH.OA.20, and either siRNA anti-CD47 or negative siRNA at 200 nM per well. Lipofectamine RNAimax was used as the positive control following the manufacturer's instructions. All conditions were performed in duplicate. OptiMEM media was used for the transfection, which lasted 24 h. Then, the cells were washed with DPBS and refreshed with growth medium. The cells were kept in the incubator to reach 72 h after transfection for giving time to the siRNA to knockdown the protein. At this point, the cells were lifted with trypsin/EDTA 0.25%, and the cell suspension was transferred to a 2 mL tube. The cells were pelleted by centrifugation and resuspended in blocking solution 5% BSA in DPBS for 30 min RT. Right after, the cells were washed and incubated for 30 min in 2% BSA with 1 μg of primary antibody against CD47 at RT. After washing the cells, the secondary antibody anti-mouse-488 was added to the cells at 10 μg/mL and incubated for 30 min. Then, the cells were transferred to flow cytometer tubes and measured with the FACS diva canto II. Mean FITC was collected from the cytometer, and relative expression of CD47 was calculated by dividing the FITC mean of siRNA CD47 by the FITC mean of negative siRNA.

3. RESULTS AND DISCUSSION

3.1. Synthesis and Characterization of Oleic Acid−Polyallylamine Substitutions. PAH is a linear polycation with primary amines previously studied as a potential nucleic acid carrier for siRNA delivery.[38,39] PAH has been also modified with cholesterol,[40,41] methylglycolate,[42] and several acrylates[43] in order to improve its delivery efficiency for siRNA and pDNA. In this work, a 17.5 kDa PAH was covalently modified with OA via amide bonds using carbodiimide chemistry. Five different molar substitutions were performed with increasing amounts of OA. Reactions were carried out starting from 100 mg of PAH and adding OA following a molar ratio of $-NH_2/-COOH$ 1:0.01, 1:0.02, 1:0.05, 1:0.1, and 1:0.2. Hereafter, the polymers obtained are named PAH.OA.1, PAH.OA.2, PAH.OA.5, PAH.OA.10, and PAH.OA.20 corresponding to the molar amount of OA added to the reaction. Polymers were purified, and the absence of free OA after purification via dialysis was confirmed by TLC (Figure S1). From ^{1}H NMR measurements (Figure 1), it can be deduced that the solubility in water of PAH decreases for the PAH substituted with the highest amount of OA. The exact amount of OA attached to PAH could not be assessed due to this solubility issue, especially for PAH.OA.20. However, an approximate degree of amine substitutions were obtained: 1, 2, 6, 14, and >14%, corresponding to PAH.OA.1, PAH.OA.2, PAH.OA.5, PAH.OA.10, and PAH.OA.20 samples, respectively. FTIR and elemental analysis confirmed the presence of OA in the polymer. Surprisingly, the percentage of oxygen seemed to decrease with increasing OA functionalization. This unexpected decrease was attributed to the water associated with PAH, which is a very hydroscopic polymer. The modification of PAH with the hydrophobic OA reduces the hydration of the polymer chains. FTIR analysis (Figure S2) showed that the 3000 cm^{-1} corresponding to the regions of $-CH_2-CH_3-$ and $-CH_2-CH_2-$ increase and sharpen with the amount of grafted OA, as well as the appearance of a peak in the 1735 cm^{-1} corresponding to the amide formed by the amines of PAH with the carboxylate groups of OA. Elemental analysis (e S1) showed that the relative carbon analysis (Table S1) showed that the relative carbon content increased gradually with the substitution of OA.

3.2. Complexation of siRNA and Carrier Evaluation. The OA-substituted polyamines complex with negatively charged nucleic acids by electrostatic interactions, forming polyplex nanoparticles (Figure 2A). Using different ratios of polymer to siRNA can largely affect the performance of the polyplexes in the delivery of siRNA to the cell cytosol. The N/P ratio is defined as the moles of nitrogen present in the polymer divided by the number of moles of phosphates present in the siRNA. Low polymer-to-siRNA ratios could result in a limited entrapment of siRNA, while large ratios may affect cell viability because of the excess of amino groups available. Four N/P ratios were tested to determine the best N/P ratio for polyplex preparation. The N/P ratios used were 2.5, 5, 10, and 15 for both PAH and OA-derived PAHs.

Unmodified free PAH is soluble in water and does not form nanoparticles. However, when it is complexed with siRNA, nanoparticles are formed with a hydrodynamic diameter of 100−150 nm depending on the N/P ratio (Figure 2B, *Z* average and Table 1). PAH substituted with OA self-forms nanoparticles in water without siRNA. Aliphatic chains of OA pending from the polymer backbone associate with hydrophobic interactions. The level of substitution impacts on the

Table 1. *Z*-Average Obtained from DLS Measurements of Polymer/siRNA Polyplexes at Different N/P Ratios[a]

	% DS OA	N/P	Z-average mean ± SD(d·nm)	PDI
PAH	0	0 (only polymer)	N/A	N/A
		2.5	123 ± 6	0.429
		5	154 ± 5	0.394
		10	141 ± 3	0.409
		15	101 ± 8	0.278
PAH.OA.1	1	0 (only polymer)	267 ± 11	0.269
		2.5	162 ± 13	0.147
		5	169 ± 5	0.123
		10	207 ± 29	0.119
		15	201 ± 11	0.133
PAH.OA.2	2	0 (only polymer)	322 ± 13	0.217
		2.5	256 ± 4	0.279
		5	198 ± 10	0.209
		10	233 ± 6	0.205
		15	215 ± 6	0.11
PAH.OA.5	6	0 (only polymer)	137 ± 2	0.405
		2.5	120 ± 18	0.264
		5	137 ± 4	0.209
		10	178 ± 7	0.405
		15	150 ± 2	0.348
PAH.OA.10	14	0 (onlypolymer)	117 ± 1	0.43
		2.5	132 ± 1	0.205
		5	123 ± 2	0.273
		10	133 ± 3	0.261
		15	131 ± 2	0.375
PAH.OA.20	>14	0 (only polymer)	147 ± 1	0.224
		2.5	122 ± 3	0.168
		5	116 ± 3	0.206
		10	136 ± 6	0.279
		15	142 ± 3	0.233

[a]N/P 0 refers to free polymer without complexation of siRNA. PDI stands for index of polydispersity.

https://doi.org/10.1021/acsabm.2c00845
ACS Appl. Bio Mater. 2023, 6, 529−542

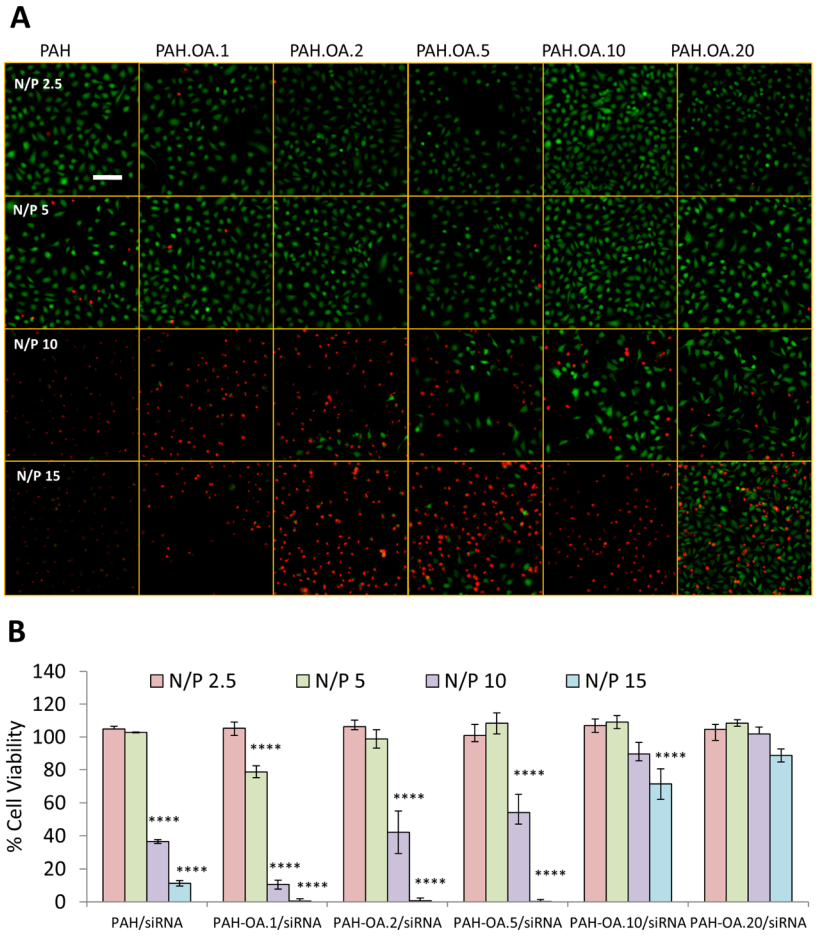

Figure 3. (A) Live/dead assay in A549 cells 24 h after transfection with polyplexes with different OA substitutions. Green staining corresponds to living cells and red to dead cells. (B) MTS assay to determine the metabolic activity of A549 cells 24 h after transfection with same polyplexes. Scale 50 μm. $n = 3$. Error bars represent standard deviation. Statistical analysis: One-way ANOVA against control nontreated cells representing 100%. *P*-valor * < 0.05, ** < 0.01, *** < 0.001, and **** < 0.0001.

size of the self-assembled structures. Low-substituted PAH (PAH.OA.1 and PAH.OA.2) results in nanoparticles with sizes around 250−350 nm. Highly substituted polymers (PAH.OA.5, PAH.OA.10, and PAH.OA.20) form structures around 150 nm (Figure 2B and Table 1).

After the addition of siRNA, the polymer reorganizes and forms assemblies of different sizes. Low-substituted PAH (PAH.OA.1 and PAH.OA.2) forms assemblies of smaller sizes, 150−250 nm, compared to the free polymer. Highly substituted polymers (PAH.OA.5, PAH.OA.10, and PAH.OA.20) form assemblies of 150 nm, same size as the nanoparticles based on the free polymer. The N/P ratio has a limited influence on the size of the nanoparticles. All N/P ratios have similar size, and its PDI is between 0.2 and 0.3 in all conditions, as observed by DLS (Table 1). When functionalized with OA, the polymer self-assembles in water to form colloids of 117 to 322 nm (see Figure 2 blue line and Table 1, only polymer). When the siRNA is complexed to the PAH-OA, a significant effect of the N/P ratio on the size of polyplexes could not be observed. This is probably because both complexation with siRNA and self-assembly of PAH-OA play a role in the formation of polyplex nanoparticles and determine the nanoparticle size. It is to note that for most of the cases, the polyplexes are smaller than the nanoparticles formed by the self-assembly of PAH-OA without complexation with siRNA. Polyplexes were previously filtered before DLS measurements to remove large aggregates. Hydrodynamic diameter measurement of the pristine dispersion showed the presence of a small amount of large aggregate. As DLS is an intensity-based measurement, these larger aggregates scattered much more light than the individual polyplexes and shielded the presence of the main population.

Transmission electron microscopy (TEM) image in Figure 2D is representative of the polyplexes formed with substituted PAH.OA.10 and siRNA at N/P ratio 5. The other PAH.OA substitutions are showed in Figure S5. Polyplexes substituted with a higher amount of OA (PAH.OA.5, PAH.OA.10, and PAH.OA.20) are round-shaped, with sizes of 12 nm in diameter, which tend to aggregate into larger structures. The smaller size measured by TEM, compared with DLS measurements, is probably due the presence of a small fraction of larger aggregates of polyplexes. DLS tends to oversize the *Z*-average. This is because a small population of large particles scatters much more light than small ones. Such differences in size between DLS and TEM data have also been found in polyplexes based in other polycations with pDNA and siRNA.[44,45] Moreover, when we consider the number distribution (Figure S3) instead of the *Z* average, the mean size of the polyplex decreases to around 50 nm for the polyplexes with the highest oleic substitutions (PAH.OA.5, PAH.OA.10, and PAH.OA.20), while for the lowest substitutions, average sizes are around 100−200 nm. These values

https://doi.org/10.1021/acsabm.2c00845
ACS Appl. Bio Mater. 2023, 6, 529−542

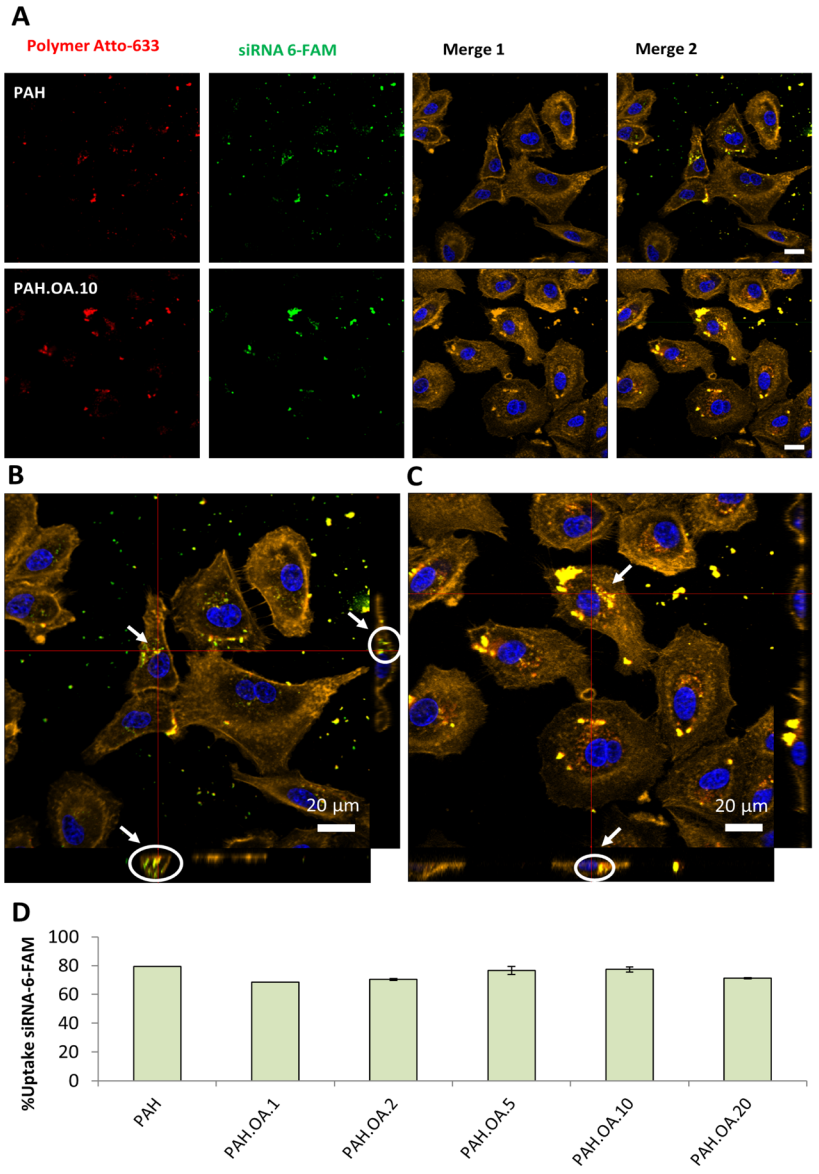

Figure 4. Confocal microscopy micrographs of A549 cells 24 h after being transfected with fluorescently labeled polyplexes PAH.OA/siRNA N/P 5. (A) PAH and PAH.OA.10 labeled with Atto-633 fluorophore emission at 635 nm (red channel) and siRNA-6-FAM emission at 520 nm (green channel). After transfection, the cells were fixed and treated with Hoescht 33342 and ActinRed. Merge 1 channel corresponds to cells with labeled actin (yellow) and nucleus (blue). Merge 2 channel corresponds to channels of siRNA, polymer, and marked cells. (B,C) Orthogonal view of merge 2 channel for PAH and PAH.OA.10, respectively. (D) Uptake of siRNA-6-FAM in A549 cells after 24 h of transfection evaluated by flow cytometry. Data represent the percentage of fluorescent cells of a total of 10,000 events.

are more in agreement with the TEM. Different substituted polymers without siRNA (Figure S4) form nanoparticles with the same round shape and similar sizes, except for free PAH that does not form complexes.

Zeta potential of PAH/siRNA polyplexes varies from +15 to +30 mV depending on the N/P ratio (Figure 2C). PAH.OA/siRNA N/P 2.5 polyplexes have negative *Z*-potential with PAH.OA 6, 14, and >14% and positive in 1 and 2% OA substitution. When the N/P ratio is higher, the *Z*-potential turns positive with values higher than for nonsubstituted PAH, from +30 to +40 mV. When siRNA is complexed to substituted PAH, the *Z*-potential is reduced by 10 mV, except for higher substitutions of OA where the *Z*-potential remains practically constant. As the degree of substitution of PAH with OA molecules increases the *Z*-potential values increase as well, despite the larger amount of amide bounds formed, which cannot be protonated as primary amines. This has also been observed for the substitution of PEI with lipids.[46] The increase in the substitution of amines by OA increases the hydrophobicity of the chains, facilitating hydrophobic interactions for the stabilization of the assemblies and polyplexes, which lead to a displacement of positive charges from the inner to outer regions of the assemblies and result in a higher zeta potential than for less-substituted polymers.[47]

The amount of siRNA encapsulated in the polyplex nanoparticles was quantified with the quant-IT ribogreen test: a fluorophore that attaches to nucleic acids when nucleic acids are free in solution but not when complexed. From the test, it was determined that PAH and PAH.OAs encapsulate more than 90% of the total siRNA (Figure 2E). Moreover, for a low N/P ratio, the same amounts of siRNA are entrapped as

https://doi.org/10.1021/acsabm.2c00845
ACS Appl. Bio Mater. 2023, 6, 529−542

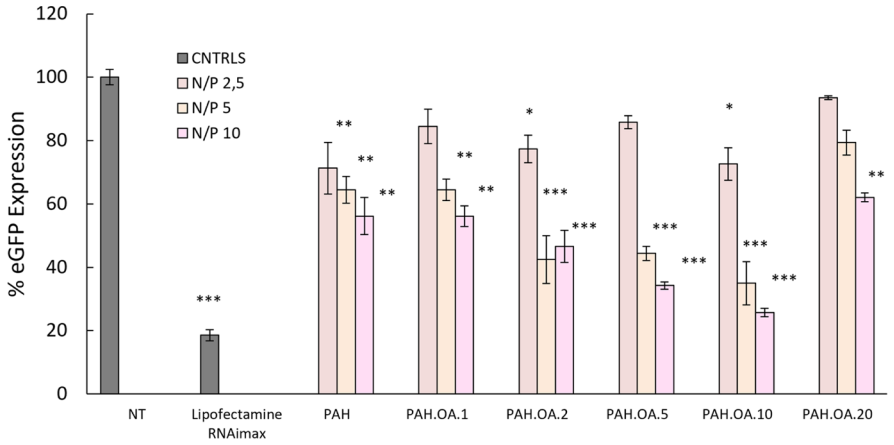

Figure 5. siRNA delivery efficiency. Expression of eGFP protein in A549-eGFP cells 96 h after being treated with siRNA anti-eGFP/PAH.OA polyplexes. Fluorescence intensity of nontreated cells represent 100%. All results are normalized to this data. $N = 3$. Error bars represent standard deviation. Data points marked with asterisks are statistically significant relative to the nontreated group. P-value * < 0.05, ** < 0.01, and *** < 0.001; t-test, single tailed.

higher N/P, meaning that there are strong interactions between the polymer and nucleic acids.

The optimal density of amine groups for a nucleic acid carrier has been widely discussed.[48−50] Amino groups in polycations condense nucleic acids but also cause cytotoxicity. Several modifications in the polycations have been performed aiming at reducing toxicological endpoints. Polyethylene glycol grafting has been frequently employed for modifying polycations, such as PEI,[51−53] PLL,[54,55] or chitosan,[56] and reducing their toxicity. Other chemical modifications of polycations such as hydrophobic modifications can be beneficial for increasing the cell viability.[57] The toxicological impact of oleic acid modification of PAH has been assessed in the pulmonary cell line A549. MTS and live/dead assays have been used to evaluate the metabolic activity and the membrane damage after being treated with the PAH.OA/siRNA polyplexes, respectively (Figure 3A,B). All polyplexes transport the same amount of siRNAs, the final concentration delivered to the cells being 200 nM. Therefore, cytotoxicity only depends on the amount of the polymer and the degree of oleic acid substitution. Live/dead experiment consists in the staining of the cells with two dyes, Calcein AM and ethidium homodimer-1 (EtdH-1). Calcein AM does not exhibit fluorescence by itself and can diffuse easily inside the cell through the plasmatic membrane. Once inside, ubiquitous esterases convert Calcein AM to calcein that has strong fluorescence activity. Good enzymatic activity inside the cell correlates with living cells. On the other hand, EtdH-1 cannot pass through an intact plasma membrane. It only enters through damaged membranes and strongly binds to DNA in the nucleus. Confocal images of A549 cells after being exposed to polyplexes are shown in Figure 3A for different N/P ratios. The MTS assay is a tetrazolium compound that is reduced by cells to the colored product formazan. The reduction is carried out by NAPDH and NADH, product molecules of metabolic activity of the cells. Absorbance of formazan is correlated with the number of living cells in the culture. The plot in Figure 3B represents absorbance data normalized to nontreated cells as 100% of viable cells. Same polymers and N/P ratios have been used as in the live/dead experiment. Low N/P ratios of 2.5 and 5, corresponding to the lowest amine exposure, are not cytotoxic for all substituted PAHs, with cell viability about 100% with respect to nontreated cells. The highest N/P ratio of 15 is cytotoxic for all substitutions except for PAH.OA.10 and PAH.OA.20. N/P 10 is cytotoxic in PAH and PAH.OA.1. However, the viability increases for higher oleic acid substitutions. At the highest N/P15, the polymers with low degrees of substitution (1% DSs) have 10% viability, while >14% DS oleic acid substitution results in 90% viability. We can conclude that oleic acid conjugations reduce PAH toxicity due to the reduced number of amines available after attachment of the oleic acid and to the self-assembly of the modified polymer, shielding a significant amount of the primary amines. Similar results were obtained with the hydrophobic modifications of PEI[58,59] that showed lower cytotoxicity because of the reduction in the number of primary amine groups. Nevertheless, large amounts of polymer remain cytotoxic. PAH.OA.10 shows low toxicity in the MTS assay for N/P 10 and 15; however, some damaged cells could be observed with the live/dead assay.

The capacity of polyplex nanoparticles to cross cell membranes was evaluated in vitro through CLSM localizing labeled siRNA and carriers inside the cell. Commercially available 6-carboxyfluorescein siRNA (siRNA-6-FAM) and Atto-633-labelled PAH via carbodiimide chemistry were used. Characterization of the labeled polymers was performed with ^{1}H NMR and FCS. NMR shows that Atto-633 is covalently attached to polymers, and FCS shows that there is no free fluorophore (Figure S6). The two fluorophores were selected as they are not overlapping in terms of their absorption/emission spectra neither to Hoescht 33342 or Actin Red which were used to stain nucleus and actin cytoskeleton, respectively.

Atto-633-labeled polymers and negative siRNA-6-FAM were complexed in RNAse-free water at N/P 5. This ratio was chosen for all PAH substitutes as a compromise between polyamine cytotoxicity and the presence of enough positive charges to promote the siRNA translocation and delivery in cytosol. A549 cells were incubated for 24 h with the polyplexes using the different substituted polymers PAH, PAH.OA.1, PAH.OA.2, PAH.OA.5, PAH.OA.10, and PAH.OA.20. Confocal images show both siRNA and polymer colocalizing inside the cells for PAH and PAH.OA.10 polyplexes in Figure 4A and for the remaining substitutions in Figure S7. To confirm that nanoparticles are internalized in the cell, z-stack images were

https://doi.org/10.1021/acsabm.2c00845
ACS Appl. Bio Mater. 2023, 6, 529−542

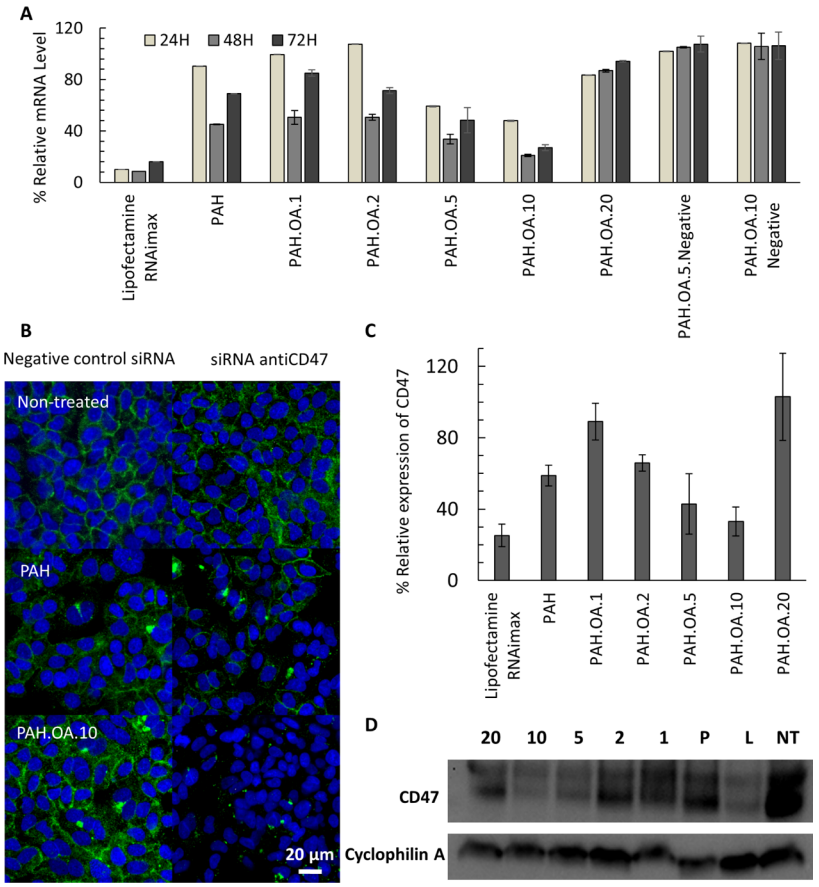

Figure 6. (A) Level of CD47 mRNA 24, 48, and 72 h after being treated with siRNA-CD47/PAH.OA N/P 5 polyplexes. mRNA was extracted and CD47 amplified by RT-qPCR. $2^{-(\Delta\Delta C_q)} \times 100$ method was used to calculate the percentage of mRNA expression relative to nontreated cells. CD47 protein expression in A549 cells 72 h after transfection with siRNA-CD47/PAH.OA N/P 5 polyplexes. (B) Immunofluorescence: treated and nontreated cells were fixed and stained with the mouse primary human CD47 antibody and secondary anti-mouse alexa fluor 488 antibody. Protein CD47 is stained in green. First column is a control corresponding to nonprimary antibody staining. Second column corresponds to transfection with negative siRNA polyplexes. Third column corresponds to siRNA antiCD47 transfection. (C) Flow cytometry of CD47-stained A549 cells. Data represented as relative expression of CD47 in percentage. siRNA-CD47 fluorescence values divided by siRNA negative fluorescence values of every transfection condition. $n = 2$. (D) Western Blot of CD47 protein. Two bands at ∼50 and ∼42 kDa. CPA as housekeeping protein 18 kDa. From right to left: Nontreated cells (NT), lipofectamine RNAimax/siRNA-CD47 (Lipo), PAH/siRNA-CD47 (PAH), PAH.OA.1/siRNA-CD47 1% OA (1), PAH.OA.2/siRNA-CD47 2% OA (2), PAH.OA.5/siRNA-CD47 6% OA (5), PAH.OA.10/siRNA-CD47 14% OA (10), PAH.OA.20/siRNA-CD47 > 14% OA (20).

conducted. Images are displayed as an orthogonal view (Figures 4B,C and S8). From confocal images and orthogonal view, it can be appreciated that polyplexes are located inside the cell as well as attached to the cell surface. The smallest polyplex nanoparticles have rapidly incorporated into the cells within 2 h, while larger particles or aggregates (>500 nm) have a slower cell uptake. As it has been reported in the literature with PEI,[15] different uptake pathways are taking place according to the size. Internalization of siRNA-6-FAM has been quantified by a flow cytometer 24 h after polyplex administration. Data represent the percentage of fluorescent cells of a total of 10,000 events. Nontreated cells have been considered 0%. Above 70% of the cells were transfected with the polyplex nanoparticles in each condition (Figure 4-D). No significant difference was found among the different PAH substitutes, meaning that oleic acid has no apparent influence on the cell membrane penetration and cell uptake. Same results have been obtained in linear PEI 2 kDa with aliphatic substitutions.[29] This could be explained because aliphatic chain is not triggering additional interactions with the cell membrane.

All synthesized oleic acid-PAH substitution can entrap siRNA and are able to deliver it inside cells. However, a strong obstacle to overcome cytosolic delivery is the escape from the endosome. To prove the delivery efficiency of our system into cancerous cells, the silencing functionality of encapsulated siRNA has been assessed. For this purpose, siRNA against GFP protein was administrated to human A549 pulmonary adenocarcinoma cells overexpressing the green fluorescence protein, A549-GFP cells. A reduction in the GFP fluorescence is indicative of a good delivery and silencing efficiency of the carrier. Cells were transfected with PAH.OA/siRNA anti-GFP at N/P 2.5, 5, and 10. N/P 15 was removed from the assay due to the cytotoxicity found in viability experiments. Cell fluorescence was measured by a flow cytometer 96 h after transfection. GFP expression is represented as a relative expression compared to nontreated cells. Figure 5 shows a low transfection efficiency for N/P 2.5 in all polymers, where the expression of GFP is above 70%. N/P 5 and N/P 10 resulted in delivery efficiency up to 50% in PAH, PAH.OA.1, and PAH.OA.2. However, it must be taken into account that these oleic substitutions are toxic at N/P 10, so the rigorous data are

https://doi.org/10.1021/acsabm.2c00845
ACS Appl. Bio Mater. 2023, 6, 529−542

taken as N/P 5. The efficacy increased in PAH.OA.5 and PAH.OA.10 reducing the GFP expression up to 60 and 70%, respectively. However, PAH.OA.20 showed lower transfection compared to the nonsubstituted PAH. Best efficiencies were obtained for PAH.OA.10 at N/P 5 and N/P 10. PAH substitution with oleic acid increases the siRNA delivery efficiency up to a certain degree. Every substitute can cross the cell membrane; however, our results hint that there are differences in the ability of escaping from the endosome. PEI aliphatic substitutions led as well to an improvement in the transfection efficiency but not to an increase in the cell uptake.[29,60] PAH.OA.10 polyplexes appear to be the best candidates to escape from the endosome and release cargo. How polymers[14] and other carriers such as lipid nanoparticles (LNPs) escape endosome is a debate. The most accepted hypothesis lies on the pKa value of the polymer or nanoparticle which should be closed to the endosomal pH, that is, 6, when acidification starts. Thus, amino groups act as a pH buffer of incoming proton during endo-lysosomal acidify cation. Proton accumulations cause osmotic swelling and compartment disruption. This effect is called "proton sponge." To elucidate how polyallylamine modified with oleic acid would overcome endo-lysosomal compartments, CLSM studies have been carried out, labelling siRNA with the Cy5 fluorophore and lysosomes with Lysotracker green (Figure S10A,B). CLSM images have been obtained at different time points: 2, 24, and 48 h after transfection. Lysosomes are the final destination of the endocytic pathway, where the acid hydrolases digest all molecules. If the labelled siRNA manages to escape from the endosome before fusing with the lysosome, we should see fluorescence from siRNA not colocalizing with the labelled lysosomes. In the CLSM images, in a majority of the cases, we observe colocalization (Figure S10A), meaning that siRNAs are present within the lysosomes. However, the presence of siRNA outside the lysosomes can be distinguished. A small leakage of siRNA molecules into the cytoplasm can be hypothesized, although most of them remain in the lysosomal interior. These data are in accordance with the studies done in LNPs, in which it is shown that only 1−2% of transfected siRNA manage to escape from the endosome[61] at early stages, although the leaked siRNA, approximately 2000 copies, are sufficient to promote gene knockdown.[62] Some works[61,63] show that endosomes remain intact after escape occurred, meaning that there are other ways to overcome the endosome barrier. The electrostatic interaction of the amines of the polymer with the endosome membrane and membrane disruption is another alternative explanation to cytosol translocation. In any case, the proof of translocation is given by the successful transfection. The siRNA cannot silence if it does not reach the cytoplasm to complex the mRNA escaping from the endosomes.

The improvement in transfection efficacy with oleic acid is probably indicative of the polymers having weaker interactions with the polyamines that lead to an easier release of the siRNAs in the cytosol. Larger substitutions of oleic acid, that is, >14%, provide more stability to the polyplexes, preventing the release of the siRNAs in the cytosol. Additionally, the decrease in the number of positive charges makes less effective the interaction of the carriers with the membrane to facilitate translocation of the polyplexes.

3.3. CD47 Silencing. CD47 is a transmembrane protein overexpressed in cancer cells and is recognized by macrophages as a "don't eat" signal.[64] Blocking the interaction between CD47 and SIRPα in macrophages will promote the phagocytosis of cancer cells as demonstrated in previous works.[34,36,65,66] To explore the potential of OA-modified PAH as a vector for siRNA involved in pulmonary cancer immunotherapy, we tested its delivery capacity against the therapeutic target gene CD47. For this purpose, mRNA expression and protein quantity of the CD47 gene were evaluated after treatment with siRNA anti-CD47 using different PAH substitutes as carriers. As in previous experiments, N/P 5 was chosen to keep the balance between transfection efficiency and cytotoxicity. mRNA levels were evaluated at 24, 48, and 72 h after transfection. Results are normalized to the control of nontreated cells after applying the delta−delta C_t method ($2^{-\Delta\Delta C_t}$). As already observed for GFP transfection, PAH.OA.10 exhibited the best reduction of mRNA levels (Figure 6A). Maximal reduction of mRNA levels takes place 48 h after transfection, and after 72 h, mRNA levels recovered slightly. To ensure that the reduction of mRNA levels is not due to an interaction of the polymer, siRNA with no silencing toward CD47 was used as the negative control. Negative control siRNA/PAH.OA.5 and PAH.OA.10 did not reduce CD47 mRNA. Knockdown of CD47 protein after release of siRNA using PAH.OA polymers was evaluated by western blot and immunofluorescence of CD47 in A549. Confocal microscopy images after immunostaining with CD47 antibodies are shown in Figure 6B for nontreated cells and cells administrated with PAH and PAH.OA.10 nanoparticles and in Figure S8 with PAH.OA.1, PAH.OA.2, PAH.OA.5, and PAH.OA.20. Left column represents the transfection with a negative control siRNA. Right column corresponds to the transfection with siRNA anti-CD47. Results show that the CD47 protein was fully expressed in the cell membrane after transfection with the negative control siRNA. However, the expression decreased with the delivery of siRNA anti-CD47, partially for PAH, PAH.OA.1, and PAH.OA.2, and mostly disappeared with PAH.OA.5 and PAH.OA.10. CD47 expression remained unchanged with PAH.OA.20. A western blot of protein CD47 after transfection with siRNA anti-CD47 is shown in Figure 6D. CPA was chosen as the endogenous gene because of good separation in molecular weight (18 kDa) with respect to CD47 (47−52 kDa). CPA expression is not changed after treatment with siRNA-CD47 polyplexes. However, some polyplexes modified the expression of CD47. PAH.OA.5 and PAH.OA.10 showed thinner and weaker bands compared to PAH, PAH.OA.1, and PAH.OA.2. These data correlate with mRNA levels (Figure 6A) and immunofluorescent images (Figures 6B and S9). Quantification of CD47 knockdown was achieved by staining A549 with the CD47 antibody and measuring fluorescence from the cells by flow cytometry. siRNA negative control and siRNA anti-CD47 were used to transfect A549 cells with the oleic acid-modified PAHs. 72 h after transfection, the cells were harvested and stained with CD47 antibodies. An isotype antibody was used as the control of the anti-CD47 antibody (data shown in Figure S11). Cells were analyzed by flow cytometry. Figure 6C shows the normalized data from CD47 fluorescence, calculated as fluorescence of CD47 treated with siRNA CD47 divided by fluorescence of CD47 treated with negative siRNA using the same polymer. For PAH.OA.10, CD47 expression was reduced to 33%, a transfection close to the 25% expression obtained with lipofectamine RNAimax considered as the positive control. PAH.OA.5 proved to be the second most effective polymer resulting in an expression of CD47 at around 43%.

https://doi.org/10.1021/acsabm.2c00845
ACS Appl. Bio Mater. 2023, 6, 529−542

PAH, PAH.OA.1 PAH.OA.2, and PAH.OA.20 did not achieve more than half protein knockdown. This data correlate with the mRNA analysis, western blot, and immunofluorescence, as well as with siRNA anti-GFP.

PAH modified with OA is a good carrier for siRNA to reduce CD47 expression in terms of transfection efficacy and toxicity. Ongoing work is focused on in vivo transfection and on exploring the inhalation route for siRNA delivery to lung cancer.

4. CONCLUSIONS

OA modification reduces positive charges in PAH without affecting the capacity of the polyamines to form complexes with siRNA while significantly reducing the cytotoxicity of the polyplexes. In addition, the degree of substitution of PAH with OA increases the silencing efficacy for GFP for intermediate substitutions, that is, PAH.OA.5 and PAH.OA.10. At higher substitutions, the transfection efficacy decreased again. A reduction of CD47 expression down to 33% of the original value is obtained for 14% substitution of OA, which is approximately half of the expression obtained for pristine PAH, that is, 60%. To conclude, OA functionalization of PAH provides a means to fine tune the charge of polyamines, improving the transfection efficacy and decreasing the toxicity, thus enhancing the therapeutical potential. The results of this work highlight the importance of charge balancing in polyamines defining toxicological endpoints, favoring complexation with nucleic acids, and facilitating nucleic acid release and translocation into the cell cytoplasm. Our results show the potential application of the carriers in therapy, particularly for the CD47 silencing in the cancer cell, which is an interesting approach to fight solid tumors by modulating cancerous cells.

■ ASSOCIATED CONTENT

Supporting Information

The Supporting Information is available free of charge at https://pubs.acs.org/doi/10.1021/acsabm.2c00845.

Materials, FTIR spectra of PAH.OA polymers; TLC; elemental analysis; DLS by number distribution; TEM images of PAH.OA assemblies and polyplexes; ^{1}H NMR and fluorescence correlation spectroscopy of labelled PAH.OA; CLSM images of the localization of labelled polyplexes; immunofluorescence microscopy; and flow cytometry data (PDF)

■ AUTHOR INFORMATION

Corresponding Authors

Damien Dupin − *CIDETEC, Basque Research and Technology Alliance (BRTA), Parque Científico y Tecnológico de Gipuzkoa, Donostia-San Sebastián 20014, Spain;* orcid.org/0000-0003-0868-9028; Phone: +34 943 30 90 22; Email: ddupin@cidetec.es

Sergio E. Moya − *CIC biomaGUNE, Basque Research and Technology Alliance (BRTA), Donostia-San Sebastián 20014, Spain;* orcid.org/0000-0002-7174-1960; Phone: +34 943 00 53 11; Email: smoya@cicbiomagune.es

Authors

Cristian Salvador − *CIC biomaGUNE, Basque Research and Technology Alliance (BRTA), Donostia-San Sebastián 20014, Spain; CIDETEC, Basque Research and Technology Alliance (BRTA), Parque Científico y Tecnológico de Gipuzkoa, Donostia-San Sebastián 20014, Spain*

Patrizia Andreozzi − *Consorzio Sistemi a Grande Interfase, Department of Chemistry 'Ugo Schiff', University of Florence, Sesto Fiorentino 50019 Florence, Italy*

Gabriela Romero − *Department of Biomedical Engineering and Chemical Engineering, The University of Texas at San Antonio, San Antonio 78249 Texas, United States;* orcid.org/0000-0001-8081-2946

Iraida Loinaz − *CIDETEC, Basque Research and Technology Alliance (BRTA), Parque Científico y Tecnológico de Gipuzkoa, Donostia-San Sebastián 20014, Spain*

Complete contact information is available at: https://pubs.acs.org/10.1021/acsabm.2c00845

Notes

The authors declare no competing financial interest.

■ ACKNOWLEDGMENTS

S.E.M. thanks the PID2020-114356RB-I00 project from the Ministry of Science and Innovation of the Government of Spain. S.E.M. and G.R. acknowledge support from the H2020 MSCA-RISE 2020 Project SUPRO-GEN, grant agreement No. 101008072. This work was performed under the Maria de Maeztu Units of Excellence Program from the Spanish State Research Agency—grant no. MDM-2017-0720. We thank Tanja Lüdtke for FCS measurements.

■ REFERENCES

(1) Zou, G. M.; Wu, W.; Chen, J.; Rowley, J. D. Duplexes of 21-Nucleotide RNAs Mediate RNA Interference in Differentiated Mouse ES Cells. *Biol. Cell* **2003**, *95*, 365−371.

(2) Gu, S.; Kay, M. A. How Do MiRNAs Mediate Translational Repression? *Silence* **2010**, *1*, 11.

(3) Caplen, N. J.; Parrish, S.; Imani, F.; Fire, A.; Morgan, R. A. Specific Inhibition of Gene Expression by Small Double-Stranded RNAs in Invertebrate and Vertebrate Systems. *Proc. Natl. Acad. Sci. U.S.A.* **2001**, *98*, 9742−9747.

(4) Hu, B.; Zhong, L.; Weng, Y.; Peng, L.; Huang, Y.; Zhao, Y.; Liang, X. J. Therapeutic SiRNA: State of the Art. *Signal Transduction Targeted Ther.* **2020**, *5*, 101.

(5) Fire, A.; Xu, S.; Montgomery, M. K.; Kostas, S. A.; Driver, S. E.; Mello, C. C. Potent and Specific Genetic Interference by Double-Stranded RNA in Caenorhabditis Elegans. *Nature* **1998**, *391*, 806−811.

(6) Akinc, A.; Maier, M. A.; Manoharan, M.; Fitzgerald, K.; Jayaraman, M.; Barros, S.; Ansell, S.; Du, X.; Hope, M. J.; Madden, T. D.; Mui, B. L.; Semple, S. C.; Tam, Y. K.; Ciufolini, M.; Witzigmann, D.; Kulkarni, J. A.; van der Meel, R.; Cullis, P. R. The Onpattro Story and the Clinical Translation of Nanomedicines Containing Nucleic Acid-Based Drugs. *Nat. Nanotechnol.* **2019**, *14*, 1084−1087.

(7) Scott, L. J. Givosiran: First Approval. *Drugs* **2020**, *80*, 335−339.

(8) Agarwal, S.; Simon, A. R.; Goel, V.; Habtemariam, B. A.; Clausen, V. A.; Kim, J. B.; Robbie, G. J. Pharmacokinetics and Pharmacodynamics of the Small Interfering Ribonucleic Acid, Givosiran, in Patients With Acute Hepatic Porphyria. *Clin. Pharmacol. Ther.* **2020**, *108*, 63−72.

(9) Turner, J. J.; Jones, S. W.; Moschos, S. A.; Lindsay, M. A.; Gait, M. J. MALDI-TOF Mass Spectral Analysis of SiRNA Degradation in Serum Confirms an RNAse A-like Activity. *Mol. Biosyst.* **2007**, *3*, 43−50.

(10) Bartlett, D. W.; Su, H.; Hildebrandt, I. J.; Weber, W. A.; Davis, M. E. Impact of Tumor-Specific Targeting on the Biodistribution and Efficacy of SiRNA Nanoparticles Measured by Multimodality in Vivo Imaging. *Proc. Natl. Acad. Sci. U.S.A.* **2007**, *104*, 15549−15554.

(11) Huang, Y.; Cheng, Q.; Ji, J. L.; Zheng, S.; Du, L.; Meng, L.; Wu, Y.; Zhao, D.; Wang, X.; Lai, L.; Cao, H.; Xiao, K.; Gao, S.; Liang, Z. Pharmacokinetic Behaviors of Intravenously Administered SiRNA in Glandular Tissues. *Theranostics* **2016**, *6*, 1528−1541.
(12) Huang, Y.; Hong, J.; Zheng, S.; Ding, Y.; Guo, S.; Zhang, H.; Zhang, X.; Du, Q.; Liang, Z. Elimination Pathways of Systemically Delivered SiRNA. *Mol. Ther.* **2011**, *19*, 381−385.
(13) Lostalé-Seijo, I.; Montenegro, J. Synthetic Materials at the Forefront of Gene Delivery. *Nat. Rev. Chem.* **2018**, *2*, 258−277.
(14) Bus, T.; Traeger, A.; Schubert, U. S. The Great Escape: How Cationic Polyplexes Overcome the Endosomal Barrier. *J. Mater. Chem. B* **2018**, *6*, 6904−6918.
(15) von Gersdorff, K.; Sanders, N. N.; Vandenbroucke, R.; De Smedt, S. C.; Wagner, E.; Ogris, M. The Internalization Route Resulting in Successful Gene Expression Depends on Both Cell Line and Polyethylenimine Polyplex Type. *Mol. Ther.* **2006**, *14*, 745−753.
(16) Cullis, P. R.; Hope, M. J. Lipid Nanoparticle Systems for Enabling Gene Therapies. *Mol. Ther.* **2017**, *25*, 1467−1475.
(17) Wang, H.; Zhang, S.; Lv, J.; Cheng, Y. Design of Polymers for SiRNA Delivery: Recent Progress and Challenges. *View* **2021**, *2*, 20200026.
(18) Kumar, L.; Verma, S.; Vaidya, B.; Gupta, V. Exosomes: Natural Carriers for SiRNA Delivery. *Curr. Pharm. Des.* **2015**, *21*, 4556−4565.
(19) Dinis Ano Bom, A. P. D. A.; da Costa Neves, P. C.; Bonacossa de Almeida, C. E. B.; Silva, D.; Missailidis, S. Aptamers as Delivery Agents of SiRNA and Chimeric Formulations for the Treatment of Cancer. *Pharm* **2019**, *11*, 684.
(20) Jiang, Y.; Huo, S.; Hardie, J.; Liang, X. J.; Rotello, V. M. Progress and Perspective of Inorganic Nanoparticle-Based SiRNA Delivery Systems. *Expert Opin. Drug Delivery* **2016**, *13*, 547−559.
(21) Siegel, D. P.; Epand, R. M. The Mechanism of Lamellar-to-Inverted Hexagonal Phase Transitions in Phosphatidylethanolamine: Implications for Membrane Fusion Mechanisms. *Biophys. J.* **1997**, *73*, 3089−3111.
(22) Rezaee, M.; Oskuee, R. K.; Nassirli, H.; Malaekeh-Nikouei, B. Progress in the Development of Lipopolyplexes as Efficient Non-Viral Gene Delivery Systems. *J. Controlled Release* **2016**, *236*, 1−14.
(23) Lampela, P.; Elomaa, M.; Ruponen, M.; Urtti, A.; Männistö, P. T.; Raasmaja, A. Different Synergistic Roles of Small Polyethylenimine and Dosper in Gene Delivery. *J. Controlled Release* **2003**, *88*, 173−183.
(24) Matsumoto, M.; Kishikawa, R.; Kurosaki, T.; Nakagawa, H.; Ichikawa, N.; Hamamoto, T.; To, H.; Kitahara, T.; Sasaki, H. Hybrid Vector Including Polyethylenimine and Cationic Lipid, DOTMA, for Gene Delivery. *Int. J. Pharm.* **2008**, *363*, 58−65.
(25) Penacho, N.; Simões, S.; de Lima, M. P. Polyethylenimine of Various Molecular Weights as Adjuvant for Transfection Mediated by Cationic Liposomes. *Mol. Membr. Biol.* **2009**, *26*, 249−263.
(26) Mahmoudi, A.; Oskuee, R.; Ramezani, M.; Malaekeh-Nikoue, B. Preparation and In-Vitro Transfection Efficiency Evaluation of Modified Cationic Liposome-Polyethyleneimine-Plasmid Nanocomplexes as a Novel Gene Carrier. *Curr. Drug Delivery* **2014**, *11*, 636−642.
(27) Yang, X.; Peng, Y.; Yu, B.; Yu, J.; Zhou, C.; Mao, Y.; Lee, L. J.; Lee, R. J. A Covalently Stabilized Lipid-Polycation-DNA (SLPD) Vector for Antisense Oligonucleotide Delivery. *Mol. Pharm.* **2011**, *8*, 709−715.
(28) Alshamsan, A.; Haddadi, A.; Incani, V.; Samuel, J.; Lavasanifar, A.; Uludağ, H. Formulation and Delivery of SiRNA by Oleic Acid and Stearic Acid Modified Polyethylenimine. *Mol. Pharm.* **2009**, *6*, 121−133.
(29) Neamnark, A.; Suwantong, O.; Remant Bahadur, K. C.; Hsu, C. Y. M.; Supaphol, P.; Uludağ, H. Aliphatic Lipid Substitution on 2 KDa Polyethylenimine Improves Plasmid Delivery and Transgene Expression. *Mol. Pharm.* **2009**, *6*, 1798−1815.
(30) Kumar, V.; Yadavilli, S.; Kannan, R. A Review on RNAi Therapy for NSCLC: Opportunities and Challenges. *Wiley Interdiscip. Rev.: Nanomed. Nanobiotechnol.* **2021**, *13*, No. e1677.
(31) June, C. H.; O'Connor, R. S.; Kawalekar, O. U.; Ghassemi, S.; Milone, M. C. CAR T Cell Immunotherapy for Human Cancer. *Science* **2018**, *359*, 1361−1365.
(32) Kim, H. S.; Kim, J. Y.; Seol, B.; Song, C. L.; Jeong, J. E.; Cho, Y. S. Directly Reprogrammed Natural Killer Cells for Cancer Immunotherapy. *Nat. Biomed. Eng.* **2021**, *5*, 1360−1376.
(33) Xiang, X.; Wang, J.; Lu, D.; Xu, X. Targeting Tumor-Associated Macrophages to Synergize Tumor Immunotherapy. *Signal Transduction Targeted Ther.* **2021**, *6*, 75.
(34) Schürch, C. M.; Roelli, M. A.; Forster, S.; Wasmer, M. H.; Brühl, F.; Maire, R. S.; Di Pancrazio, S.; Ruepp, M. D.; Giger, R.; Perren, A.; Schmitt, A. M.; Krebs, P.; Charles, R. P.; Dettmer, M. S. Targeting CD47 in Anaplastic Thyroid Carcinoma Enhances Tumor Phagocytosis by Macrophages and Is a Promising Therapeutic Strategy. *Thyroid* **2019**, *29*, 979−992.
(35) Liu, R.; Wei, H.; Gao, P.; Yu, H.; Wang, K.; Fu, Z.; Ju, B.; Zhao, M.; Dong, S.; Li, Z.; He, Y.; Huang, Y.; Yao, Z. CD47 Promotes Ovarian Cancer Progression by Inhibiting Macrophage Phagocytosis. *Oncotarget* **2017**, *8*, 39021−39032.
(36) Wang, Y.; Xu, Z.; Guo, S.; Zhang, L.; Sharma, A.; Robertson, G. P.; Huang, L. Intravenous Delivery of SiRNA Targeting CD47 Effectively Inhibits Melanoma Tumor Growth and Lung Metastasis. *Mol. Ther.* **2013**, *21*, 1919−1929.
(37) Wu, J.; Li, Z.; Yang, Z.; Guo, L.; Zhang, Y.; Deng, H.; Wang, C.; Feng, M. A Glutamine-Rich Carrier Efficiently Delivers Anti-CD47 SiRNA Driven by a "Glutamine Trap" to Inhibit Lung Cancer Cell Growth. *Mol. Pharm.* **2018**, *15*, 3032−3045.
(38) Andreozzi, P.; Diamanti, E.; Py-Daniel, K. R.; Cáceres-Vélez, P. R.; Martinelli, C.; Politakos, N.; Escobar, A.; Muzi-Falconi, M.; Azevedo, R.; Moya, S. E. Exploring the PH Sensitivity of Poly(Allylamine) Phosphate Supramolecular Nanocarriers for Intracellular SiRNA Delivery. *ACS Appl. Mater. Interfaces* **2017**, *9*, 38242−38254.
(39) Di Silvio, D.; Martínez-Moro, M.; Salvador, C.; de los Angeles Ramirez, M.; Caceres-Velez, P. R.; Ortore, M. G.; Dupin, D.; Andreozzi, P.; Moya, S. E. Self-Assembly of Poly(Allylamine)/SiRNA Nanoparticles, Their Intracellular Fate and SiRNA Delivery. *J. Colloid Interface Sci.* **2019**, *557*, 757−766.
(40) Guo, J.; O'Mahony, A. M.; Cheng, W. P.; O'Driscoll, C. M. Amphiphilic Polyallylamine Based Polymeric Micelles for SiRNA Delivery to the Gastrointestinal Tract: In Vitro Investigations. *Int. J. Pharm.* **2013**, *447*, 150−157.
(41) Oskuee, R. K.; Ramezanpour, M.; Gholami, L.; Malaekeh-Nikouei, B. Cholesterol Improves the Transfection Efficiency of Polyallylamine as a Non-Viral Gene Delivery Vector. *Braz. J. Pharm. Sci.* **2017**, *53*, No. e00140.
(42) Boussif, O.; Delair, T.; Brua, C.; Veron, L.; Pavirani, A.; Kolbe, H. V. J. Synthesis of Polyallylamine Derivatives and Their Use as Gene Transfer Vectors in Vitro. *Bioconjugate Chem.* **1999**, *10*, 877−883.
(43) Oskuee, R. K.; Mahmoudi, A.; Gholami, L.; Rahmatkhah, A.; Malaekeh-Nikouei, B. Cationic Liposomes Modified with Polyallylamine as a Gene Carrier: Preparation, Characterization and Transfection Efficiency Evaluation. *Adv. Pharm. Bull.* **2016**, *6*, 515−520.
(44) Shi, J.; Schellinger, J. G.; Johnson, R. N.; Choi, J. L.; Chou, B.; Anghel, E. L.; Pun, S. H. Influence of Histidine Incorporation on Buffer Capacity and Gene Transfection Efficiency of HPMA-Co-Oligolysine Brush Polymers. *Biomacromolecules* **2013**, *14*, 1961.
(45) Troiber, C.; Kasper, J. C.; Milani, S.; Scheible, M.; Martin, I.; Schaubhut, F.; Küchler, S.; Rädler, J.; Simmel, F. C.; Friess, W.; Wagner, E. Comparison of Four Different Particle Sizing Methods for SiRNA Polyplex Characterization. *Eur. J. Pharm. Biopharm.* **2013**, *84*, 255−264.
(46) Remant Bahadur, K. C.; Landry, B.; Aliabadi, H. M.; Lavasanifar, A.; Uludağ, H. Lipid Substitution on Low Molecular Weight (0.6-2.0 KDa) Polyethylenimine Leads to a Higher Zeta Potential of Plasmid DNA and Enhances Transgene Expression. *Acta Biomater.* **2011**, *7*, 2209−2217.

https://doi.org/10.1021/acsabm.2c00845
ACS Appl. Bio Mater. 2023, 6, 529−542

(47) Simon, M.; Wittmar, M.; Bakowsky, U.; Kissel, T. Self-Assembling Nanocomplexes from Insulin and Water-Soluble Branched Polyesters, Poly[(Vinyl-3-(Diethylamino)-Propylcarbamate-Co-(Vinyl Acetate)-Co-(Vinyl Alcohol)]-Graft-Poly(L-Lactic Acid): A Novel Carrier for Transmucosal Delivery of Peptides. *Bioconjugate Chem.* **2004**, *15*, 841−849.
(48) Putnam, D.; Gentry, C. A.; Pack, D. W.; Langer, R. Polymer-Based Gene Delivery with Low Cytotoxicity by a Unique Balance of Side-Chain Termini. *Proc. Natl. Acad. Sci. U.S.A.* **2001**, *98*, 1200−1205.
(49) Paul, A.; Eun, C. J.; Song, J. M. Cytotoxicity Mechanism of Non-Viral Carriers Polyethylenimine and Poly-l-Lysine Using Real Time High-Content Cellular Assay. *Polymer* **2014**, *55*, 5178−5188.
(50) Clamme, J. P.; Azoulay, J.; Mély, Y. Monitoring of the Formation and Dissociation of Polyethylenimine/DNA Complexes by Two Photon Fluorescence Correlation Spectroscopy. *Biophys. J.* **2003**, *84*, 1960−1968.
(51) Petersen, H.; Fechner, P. M.; Martin, A. L.; Kunath, K.; Stolnik, S.; Roberts, C. J.; Fischer, D.; Davies, M. C.; Kissel, T. Polyethylenimine-Graft-Poly(Ethylene Glycol) Copolymers: Influence of Copolymer Block Structure on DNA Complexation and Biological Activities as Gene Delivery System. *Bioconjugate Chem.* **2002**, *13*, 845−854.
(52) Hibbitts, A. J.; Ramsey, J. M.; Barlow, J.; MacLoughlin, R.; Cryan, S. A. In Vitro and in Vivo Assessment of Pegylated Pei for Anti-Il-8/Cxcl-1 Sirna Delivery to the Lungs. *Nanomaterials* **2020**, *10*, 1248.
(53) Ke, X.; Shelton, L.; Hu, Y.; Zhu, Y.; Chow, E.; Tang, H.; Santos, J. L.; Mao, H. Q. Surface-Functionalized PEGylated Nanoparticles Deliver Messenger RNA to Pulmonary Immune Cells. *ACS Appl. Mater. Interfaces* **2020**, *12*, 35835−35844.
(54) Zhou, Q.; Xiang, J.; Hao, L.; Xu, X.; Zhou, Z.; Tang, J.; Ping, Y.; Shen, Y. Polyplex Nanovesicles of Single Strand Oligonucleotides for Efficient Cytosolic Delivery of Biomacromolecules. *Nano Today* **2021**, *39*, 101221.
(55) Ye, Z.; Abdelmoaty, M. M.; Ambardekar, V. V.; Curran, S. M.; Dyavar, S. R.; Arnold, L. L.; Cohen, S. M.; Kumar, D.; Alnouti, Y.; Coulter, D. W.; Singh, R. K.; Vetro, J. A. Preliminary Preclinical Study of Chol-DsiRNA Polyplexes Formed with PLL[30]-PEG[5K] for the RNAi-Based Therapy of Breast Cancer. *Nanomedicine* **2021**, *33*, 102363.
(56) Prakash, M.; Tomaro-Duchesneau, C.; Shyamali Saha, S.; Kahouli, I.; Malhotra, S. Development and Characterization of Chitosan-PEG-TAT Nanoparticles for the Intracellular Delivery of SiRNA. *Int. J. Nanomed.* **2013**, *8*, 2041−2052.
(57) Liu, Z.; Zhang, Z.; Zhou, C.; Jiao, Y. Hydrophobic Modifications of Cationic Polymers for Gene Delivery. *Prog. Polym. Sci.* **2010**, *35*, 1144−1162.
(58) Tian, H.; Xiong, W.; Wei, J.; Wang, Y.; Chen, X.; Jing, X.; Zhu, Q. Gene Transfection of Hyperbranched PEI Grafted by Hydrophobic Amino Acid Segment PBLG. *Biomaterials* **2007**, *28*, 2899−2907.
(59) Thomas, M.; Klibanov, A. M. Enhancing Polyethylenimine's Delivery of Plasmid DNA into Mammalian Cells. *Proc. Natl. Acad. Sci. U.S.A.* **2002**, *99*, 14640−14645.
(60) Aliabadi, H. M.; Landry, B.; Bahadur, R. K.; Neamnark, A.; Suwantong, O.; Uludağ, H. Impact of Lipid Substitution on Assembly and Delivery of SiRNA by Cationic Polymers. *Macromol. Biosci.* **2011**, *11*, 662−672.
(61) Gilleron, J.; Querbes, W.; Zeigerer, A.; Borodovsky, A.; Marsico, G.; Schubert, U.; Manygoats, K.; Seifert, S.; Andree, C.; Stöter, M.; Epstein-Barash, H.; Zhang, L.; Koteliansky, V.; Fitzgerald, K.; Fava, E.; Bickle, M.; Kalaidzidis, Y.; Akinc, A.; Maier, M.; Zerial, M. Image-Based Analysis of Lipid Nanoparticle-Mediated SiRNA Delivery, Intracellular Trafficking and Endosomal Escape. *Nat. Biotechnol.* **2013**, *31*, 638−646.
(62) Wittrup, A.; Ai, A.; Liu, X.; Hamar, P.; Trifonova, R.; Charisse, K.; Manoharan, M.; Kirchhausen, T.; Lieberman, J. Visualizing Lipid-Formulated SiRNA Release from Endosomes and Target Gene Knockdown. *Nat. Biotechnol.* **2015**, *33*, 870−876.
(63) Rehman, Z. U.; Hoekstra, D.; Zuhorn, I. S. Mechanism of Polyplex- and Lipoplex-Mediated Delivery of Nucleic Acids: Real-Time Visualization of Transient Membrane Destabilization without Endosomal Lysis. *ACS Nano* **2013**, *7*, 3767−3777.
(64) Huang, C. Y.; Ye, Z. H.; Huang, M. Y.; Lu, J. J. Regulation of CD47 Expression in Cancer Cells. *Transl. Oncol.* **2020**, *13*, 100862.
(65) Willingham, S. B.; Volkmer, J. P.; Gentles, A. J.; Sahoo, D.; Dalerba, P.; Mitra, S. S.; Wang, J.; Contreras-Trujillo, H.; Martin, R.; Cohen, J. D.; Lovelace, P.; Scheeren, F. A.; Chao, M. P.; Weiskopf, K.; Tang, C.; Volkmer, A. K.; Naik, T. J.; Storm, T. A.; Mosley, A. R.; Edris, B.; Schmid, S. M.; Sun, C. K.; Chua, M. S.; Murillo, O.; Rajendran, P.; Cha, A. C.; Chin, R. K.; Kim, D.; Adorno, M.; Raveh, T.; Tseng, D.; Jaiswal, S.; Enger, P. Ø.; Steinberg, G. K.; Li, G.; So, S. K.; Majeti, R.; Harsh, G. R.; van de Rijn, M. D.; Teng, N. N. H.; Sunwoo, J. B.; Alizadeh, A. A.; Clarke, M. F.; Weissman, I. L. The CD47-Signal Regulatory Protein Alpha (SIRPa) Interaction Is a Therapeutic Target for Human Solid Tumors. *Proc. Natl. Acad. Sci. U.S.A.* **2012**, *109*, 6662−6667.
(66) Zhao, H.; Wang, J.; Kong, X.; Li, E.; Liu, Y.; Du, X.; Kang, Z.; Tang, Y.; Kuang, Y.; Yang, Z.; Zhou, Y.; Wang, Q. CD47 Promotes Tumor Invasion and Metastasis in Non-Small Cell Lung Cancer. *Sci. Rep.* **2016**, *6*, 29719.

https://doi.org/10.1021/acsabm.2c00845
ACS Appl. Bio Mater. 2023, 6, 529−542